Catalysis Today xxx (2019) xxx-xxx

Contents lists available at ScienceDirect

Catalysis Today

journal homepage: www.elsevier.com

Synthesis of Ru-based catalysts for CO_2 methanation and experimental assessment of intraporous transport limitations

Alessandro Porta[a], Leonardo Falbo[a], Carlo Giorgio Visconti[a,*], Luca Lietti[a,*], Claudia Bassano[b], Paolo Deiana[b]

[a] Dipartimento di Energia, Politecnico Di Milano, via Lambruschini 4, Milano, 20156, Italy
[b] ENEA, via Anguillarese 301, Santa Maria di Galeria, Roma, 00123, Italy

ARTICLE INFO

Keywords:
Sabatier reaction
CO_2 methanation
Power-to-Gas
$Ru/\gamma\text{-}Al_2O_3$
Eggshell catalysts
Internal diffusional limitations

ABSTRACT

Aiming at the optimization of the efficiency of the CO_2 methanation process at industrially relevant conditions on Ru/Al_2O_3 catalysts, the effect of the size of the catalytic pellet on the catalyst performance has been investigated. For this purpose, $\gamma\text{-}Al_2O_3$ spheres of various diameters (100, 800 and 2300 μm) have been impregnated so to achieve a 0.5 wt. % Ru loading. Interestingly, the dry impregnation method has led to the preparation of eggshell catalysts on supports bigger than 100 μm. This indicates a strong interaction between the $\gamma\text{-}Al_2O_3$ support and the Ru precursor, which is thus deposited only on the outer shell of the spherical pellets. By changing this interaction by tuning the acidity of the impregnating solution with an inorganic acid, it is possible to effectively control the thickness of the catalytic layer, and homogeneously impregnated pellets can eventually be obtained. The impregnated pellets have been tested in process conditions of industrial interest for CO_2 methanation, under kinetically controlled regime (i.e. after crushing and sieving). No differences in CO_2 conversion nor in CH_4 selectivity have been observed between the powdered homogeneously impregnated pellet and the powdered eggshell pellet when HNO_3 is used to modify the pH of the impregnating solution, indicating that the acid introduction does not affect the catalyst performance. Subsequently, homogeneously impregnated pellets have been tested to assess the role of internal diffusional limitations. No significant differences in the catalyst activity have been observed when varying the dimension of the pellets, indicating the absence of relevant intraporous diffusional limitations with a Ru loading of 0.5 wt. %. Evidences have been collected also on the role of Cl ions remaining on the catalyst surface when using $RuCl_3$ as precursor and/or HCl as acidifying compound.

1. Introduction

The continuous exploitation of fossil fuels is causing an increase in the concentration of CO_2 in the atmosphere, resulting in a sensible temperature increase due to the well-known greenhouse effect. With the challenging purpose of limiting the temperature increase, recent focus has been put on Carbon Capture and Utilization (CCU) technologies [1], possibly exploiting excess renewable energy, coming from fluctuating sources such as wind and sunlight [2]. In this way, it is possible to effectively store renewable energy by converting "waste" captured CO_2 into valuable products. One example of these technologies is the Power-to-Gas (PtG) process. According to this technology, renewable electricity is used to electrolyze water, obtaining a H_2 stream, which is then fed to a catalytic reactor together with captured CO_2 to produce Synthetic Natural Gas (SNG) through the Sabatier reaction (Eq. 1):

$$CO_2 + 4\,H_2 \rightarrow CH_4 + 2\,H_2O \quad \Delta H^{\circ}_R\,(298\,K) = -165\,kJ/mol \qquad (1)$$

Once pressurized and separated from the water generated by the reaction, the resulting SNG can be directly injected into the existing gas grid or gas storages and can be easily utilized in the well-established infrastructure and conversion systems.

The PtG technology is currently implemented at pilot scale, relying on technologies mainly based on nickel catalysts [3]. Indeed, the Sabatier reaction has been widely studied on various transition metals, but nickel is able to provide sufficiently high activity and selectivity to CH_4 at a relatively low cost [4]. On the contrary, ruthenium-based catalysts have been less considered for this process so far, mainly due to the higher cost of the noble metal. However, some advantages of ruthenium have been pointed out: Ru is more resistant than Ni in oxidizing atmospheres, it shows a higher sulphur resistance and it is less prone to

* Corresponding authors.
Email addresses: carlo.visconti@polimi.it (C.G. Visconti); luca.lietti@polimi.it (L. Lietti)

https://doi.org/10.1016/j.cattod.2019.01.042
Received 5 October 2018; Received in revised form 4 January 2019; Accepted 14 January 2019
Available online xxx
0920-5861/ © 2019.

UNCORRECTED PROOF

Table 1
Morphological characterization of the commercial alumina supports.

	S_{BET} [$m^2 g^{-1}$]	V_{pore} [$cm^3 g^{-1}$]	$d_{pore\ avg.}$ [nm]
100 μm	191	0.49	10.2
800 μm	171	0.47	10.9
2300 μm	194	0.49	10.1

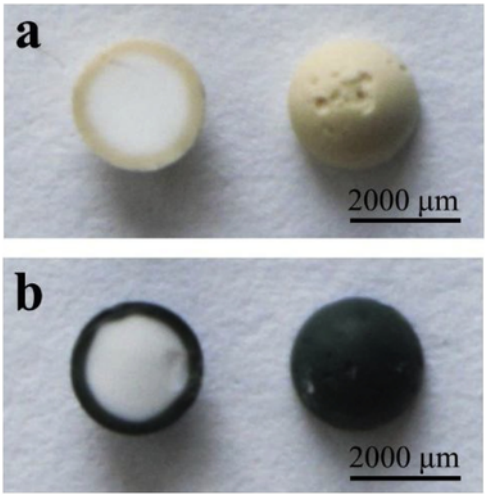


Fig. 1. Cross-section and top view of 2300 μm γ-Al_2O_3 spheres impregnated with a $Ru(NO)(NO_3)_3$ solution to obtain a nominal loading of 0.5 wt. % of Ru. a) dried at 120 °C; b) calcined at 400 °C.

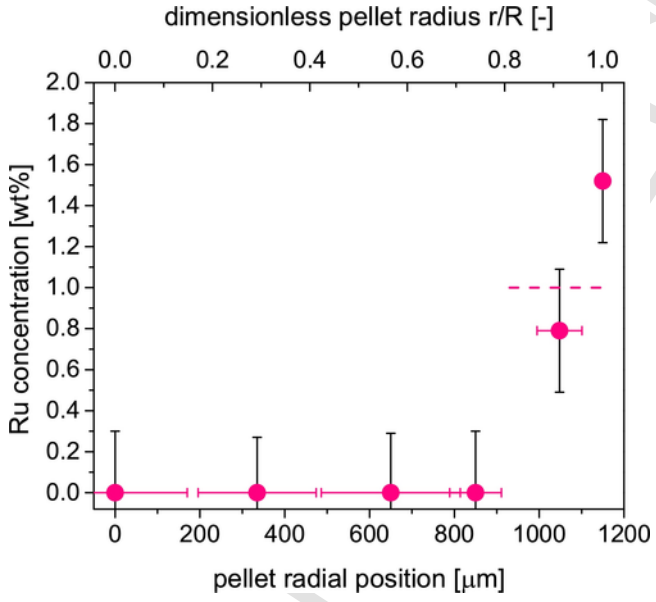


Fig. 2. SEM/EDX analysis result for the eggshell sample prepared from the $Ru(NO)(NO_3)_3$ precursor. The dotted line indicates the expected average concentration value in the active shell. Radial position 0 is located at the center of the pellet.

deactivation due to carbon deposition [3,4]. Furthermore, ruthenium catalysts are better suited than nickel catalysts for low temperature applications, due to their higher intrinsic activity [5]. Indeed, operating the reactor at temperatures lower than 400 °C, the thermodynamic equilibrium of the process further favors the products, reaching high CO_2 conversions per-pass also at low operating pressure. Furthermore, Ru-based catalysts show a very high selectivity towards methane and a very low selectivity towards CO and C_{2+} hydrocarbons [6,7]. For this reason, a possible operating solution could also be the use of both catalytic systems: a first Ni-catalyzed step followed by an additional Ru-catalyzed step to increase the CH_4 concentration in order to meet the stringent specifications required for the direct injection in the gas grid of the produced SNG.

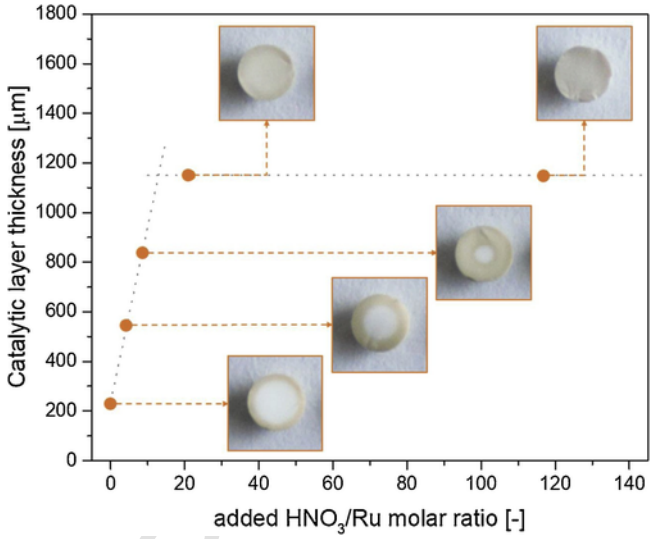


Fig. 3. Effect of the acid/metal molar ratio on the active layer thickness for a 0.5 wt% Ru/Al_2O_3 catalyst of 2300 μm prepared from $Ru(NO)(NO_3)_3$.

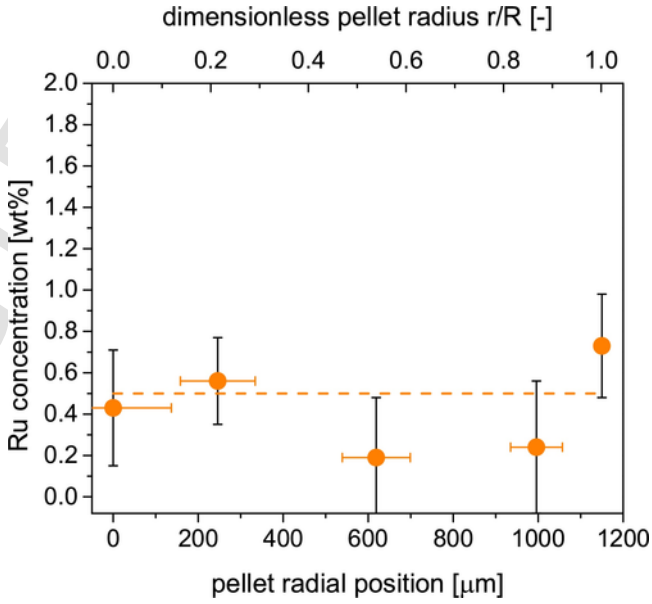


Fig. 4. SEM/EDX analysis result for the homogeneously impregnated sample prepared from $Ru(NO)(NO_3)_3$ + HNO_3 solution (HNO_3/Ru = 117). The dotted line indicates the expected concentration value in the catalyst pellet.

The Sabatier reaction is highly exothermic and it is thermodynamically limited at high temperatures; hence heat management plays a crucial role in reactor design [5]. Adiabatic fixed bed reactors operating in cascade have been proposed, alternated with heat exchangers in order to remove the heat generated by the reaction. These concepts are unsuitable for unsteady operation, due to the possible formation of hotspot upon load variations [3]. To enhance the thermal management of the reaction, the use of catalysts directly washcoated onto a heat exchanger reactor [8], or onto high conductive substrates such as metallic foams or honeycomb monoliths has been proposed [9–11]. However, these solutions are limited by the catalyst inventory and require extremely active catalysts to ensure satisfactory CH_4 yields. Another possibility is represented by externally cooled randomly packed fixed

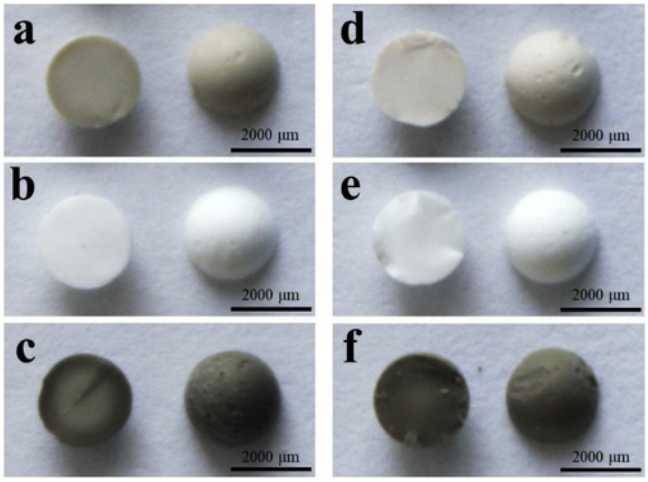


Fig. 5. 2300 μm 0.5% Ru/Al_2O_3 prepared from $Ru(NO)(NO_3)_3$ + HNO_3 solutions.HNO_3/Ru = 20: a) dried at 120 °C; b) calcined at 400 °C; c) reduced at 400 °C.HNO_3/Ru = 117: d) dried at 120 °C; e) calcined at 400 °C; f) reduced at 400 °C.

bed reactors, which are characterized by less severe temperature gradients with respect to adiabatic fixed beds, thus leading also to a relatively higher flexibility of the operative conditions.

In order to effectively operate in a fixed bed configuration, a trade-off between catalyst activity and pressure drops along the reactor must be found. Indeed, big catalyst pellets may cause low pressure drops but can at the same time limit the catalytic activity or affect the expected process selectivity due to heat and/or mass transfer limitations. On the contrary, small catalyst particles may grant a controlling kinetic regime, at the expenses of strong pressure gradients along the catalytic bed.

A possible compromise between these two alternatives is provided by eggshell catalysts. In these catalytic systems the active phase is located only in the outer layer of the pellets, thus effectively shortening the diffusional pathway inside the catalyst while still getting the advantages of working with big particle sizes.

In order to assess the critical diffusion length over which internal mass transfer limitations may affect the catalyst performance, in this work γ-Al_2O_3 spherical pellets of various diameters have been impregnated with 0.5 wt. % of ruthenium and subsequently tested as such or in their powdered form in CO_2 methanation at industrially relevant process conditions.

2. Experimental

2.1. Catalyst preparation and characterization

Commercial γ-Al_2O_3 micro-spheres (Sasol Puralox®) with diameters of 2300, 800 and 100 μm were used as supports. Surface area, pore volume and mean pore diameter were determined by N_2 adsorption-desorption isotherms at 77 K using the BET technique, using a Micromeritics Tristar 3000 instrument. Prior to the analysis, each sample was powdered and evacuated at 120 °C for 3 h. The measured morphological properties, listed in Table 1, are similar for the three supports, indicating a surface area between 171 and 194 m^2/g and a pore volume between 0.47 and 0.49 cm^3/g, thus resulting in pores with average diameters between 10 and 11 nm.

Ruthenium (III) chloride hydrate (39 wt. % Ru, Johnson Matthey) and a Ruthenium (III) nitrosyl nitrate solution (1.4 wt. % Ru, Alfa Aesar) were used as precursors of the active phase.

All catalysts were prepared by impregnation. The ruthenium concentration in the impregnating solution was set to obtain a nominal metal loading of 0.5 wt %, and a 50% volume excess of the impregnating solution with respect to the alumina pore volume was used, thus obtaining a Ru concentration in the impregnating solution equal to 0.0676 M. In some preparations, HNO_3 (65 wt. %, Honeywell) and HCl (37 wt. %, Honeywell) were used to dilute the impregnating solution. The alumina supports (which had previously been dried for 2 h at 120 °C) have been contacted with the solution and stirred at room temperature until the evaporation of the excess volume, i.e. when the incipient wetness conditions were reached. The samples were subsequently dried overnight at 120 °C.

The thickness of the active layer was measured by optical microscopy (Leica DMLM, equipped with Leica application suite for digital acquisition). Ten pellets for each batch were cut in half using a razor blade and four shell thickness measurements were taken for each half and then averaged.

Qualitative concentration profiles along the dried catalyst pellets were obtained using a scanning electron microscope (SEM) (Zeiss Evo50 EP) equipped with an energy dispersive X-ray spectrometer (EDX) (Oxford Inca Energy 200 - Pentafet LZ4). The samples were coated with a gold film prior to the analysis.

High-resolution transmission electron microscopy (HR-TEM) imaging was performed on selected catalyst using a Zeiss LIBRA 200FE analytical transmission electron microscope, equipped with 200 kV FEG. The dispersion of the metallic phase was also investigated by H_2 chemisorption experiments using a Micromeritics Thermoquest TP-

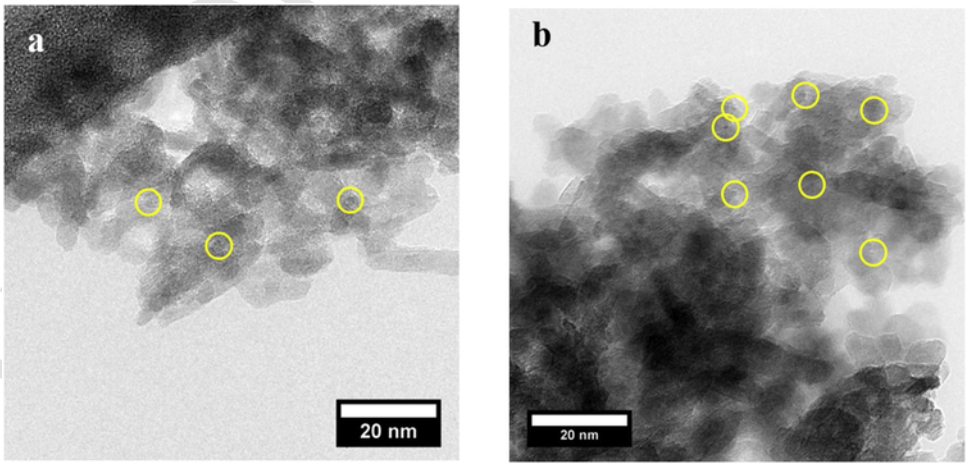


Fig. 6. TEM images of 2300 μm 0.5% Ru/Al_2O_3 prepared from $Ru(NO)(NO_3)_3$.a) eggshell configuration (HNO_3/Ru = 0) b) homogeneous sample (HNO_3/Ru = 117).

UNCORRECTED PROOF

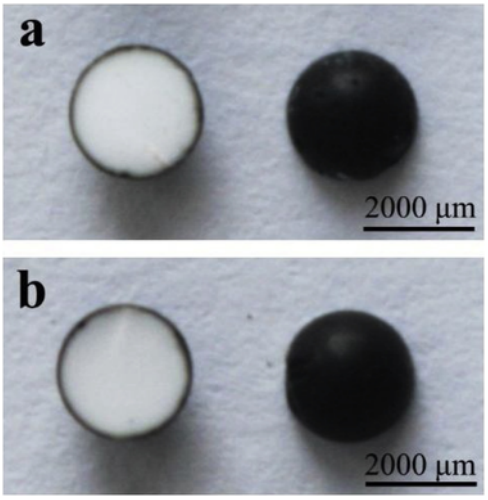


Fig. 7. 2300 µm γ-Al_2O_3 spheres impregnated with a $RuCl_3$ solution to obtain a nominal loading of 0.5 wt. % of Ru. a) dried at 120 °C; b) calcined at 400 °C.

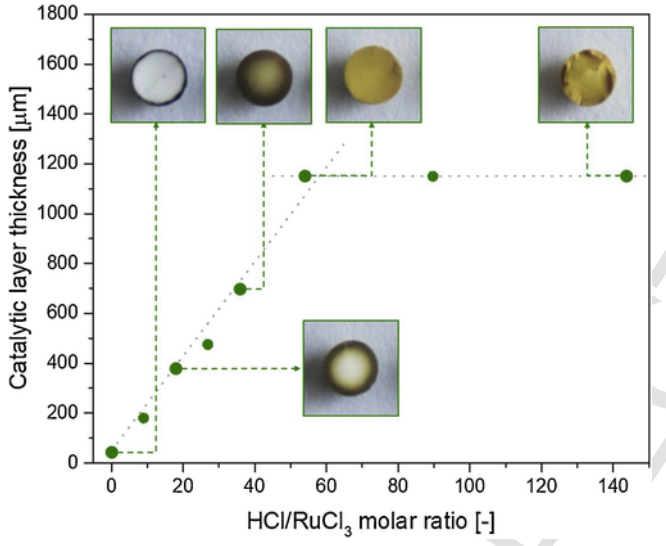


Fig. 8. Effect of the acid/metal molar ratio on the active layer thickness for a 0.5 wt% Ru/Al_2O_3 catalyst of 2300 µm prepared from $RuCl_3$.

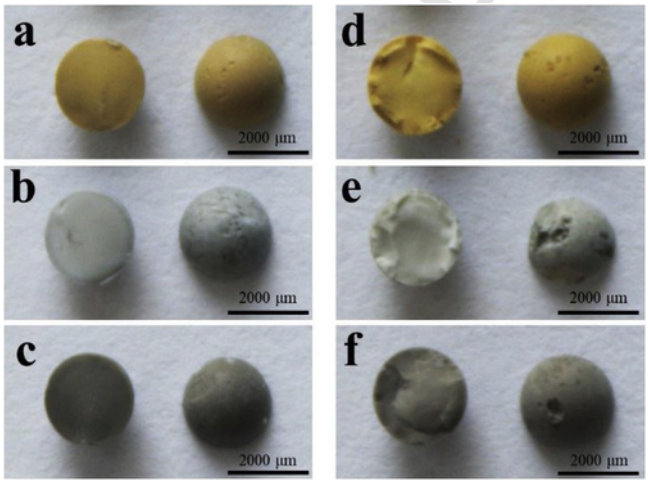


Fig. 9. 2300 µm 0.5% Ru/Al_2O_3 prepared from $RuCl_3$ + HCl solutions.HCl/Ru = 53: a) dried at 120 °C; b) calcined at 400 °C; c) reduced at 400 °C.HCl/Ru = 143: d) dried at 120 °C; e) calcined at 400 °C; f) reduced at 400 °C.

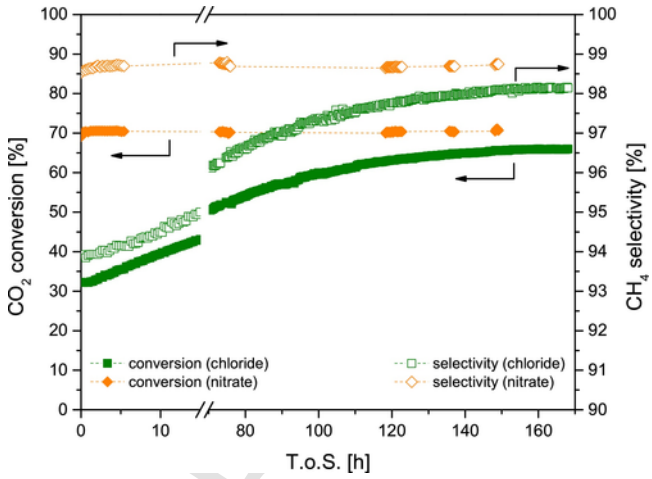


Fig. 10. Conditioning transient for 100 µm samples prepared from nitrate and chloride precursor.Process conditions: P = 0 barg, T = 350 °C, H_2/CO_2 = 3.9 mol/mol, GHSV = 5 L(STP)/h/g_{cat}.

DRO1100 instrument, equipped with a thermal conductivity detector (TCD). To this aim, 300 mg of dried catalyst were loaded in a quartz reactor and reduced in situ in H_2 flow at 400 °C for 3 h (heating rate 2 °C/min). The reduction was followed by a purge in Ar flow at the same temperature for 2 h. The catalyst was then cooled down to 100 °C and exposed to successive H_2 pulses. The metallic Ru dispersion (D) was evaluated from the amount of chemisorbed H_2 (mol_{H2}^{chemi}), assuming a complete reduction of the Ru present in the sample (mol_{Ru}^{tot}) and a Ru:H chemisorption stoichiometry equal to 1 [12–15], according to equation 2:

$$D = 2 \bullet \frac{mol_{H2}^{chemi}}{mol_{Ru}^{tot}} \quad (2)$$

2.2. Catalytic activity tests

Activity tests have been performed on the dried catalyst samples, which have been reduced in situ prior to admit the reactants in the reactor. This choice was based on the evidence reported in the literature of a detrimental effect of the calcination/reduction treatment on the active phase dispersion of supported ruthenium catalysts. Chin et al. [16] have reported a severe sintering for 1 wt. % Ru/Al_2O_3 and Ru/SiO_2 samples when subjected to oxidative treatment before the reduction. Indeed, in the case of alumina-supported sample, these authors found a drastic decrease of Ru° dispersion for the sample calcined before reduction. Similar effects have been observed in the case of Ru/SiO_2 catalysts prepared from $RuCl_3$ by Koopman et al. [17] and in the case of a zeolite A-supported ruthenium catalyst prepared from $Ru(NH_3)_6Cl_3$ by Wellenbuscher et al. [18]. These authors concluded that the oxidation treatment leads to the disruption of the linkages between support and active phase, that rapidly sinters upon reduction.

The prepared catalysts, loaded in a quartz fixed-bed reactor (I.D. 1.1 cm, length 23 cm) placed into an electric tubular furnace, were tested in CO_2 methanation in a fully-automated a lab-scale rig operating 24/7. The gaseous mixture leaving the reactor was sent to a cooler followed by a cold trap to condense the produced water. The dried stream was analyzed with an on-line gas chromatograph (Agilent, 6890) equipped with two wide-bore columns each connected to a thermal conductivity detector (TCD) to quantify the concentrations of H_2, N_2, CH_4, CO, CO_2 and C_2-C_5 hydrocarbons using an inert tracer (i.e. Ar) as internal standard. Ethylene and C_{3+} hydrocarbons were never detected, while small amounts of ethane were detected at low temperatures. The accuracy of the analysis was evaluated through carbon bal-

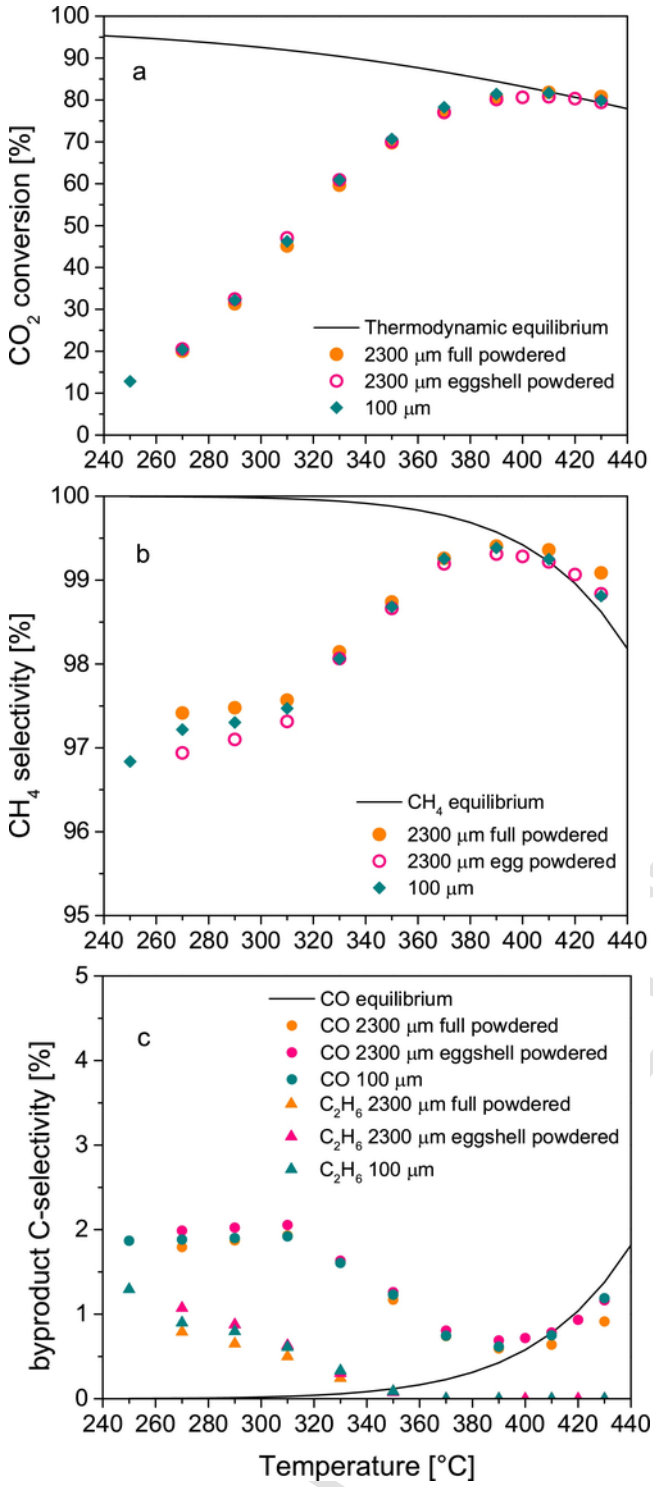


Fig. 11. CO_2 conversion (a), CH_4 selectivity (b) and CO/C_2H_6 selectivity (c) as a function of temperature for 0.5 wt. % Ru powdered catalysts obtained from 2300 μm eggshell (HNO_3/Ru = 0) and homogeneously impregnated microspheres (HNO_3/Ru = 117). 100 μm sample (HNO_3/Ru = 0) is reported for comparison. All catalysts have been impregnated with a $Ru(NO)(NO_3)_3$ solution.Process conditions: P = 0 barg, H_2/CO_2 = 3.9 mol/mol, GHSV = 5 L(STP)/h/g_{cat}.

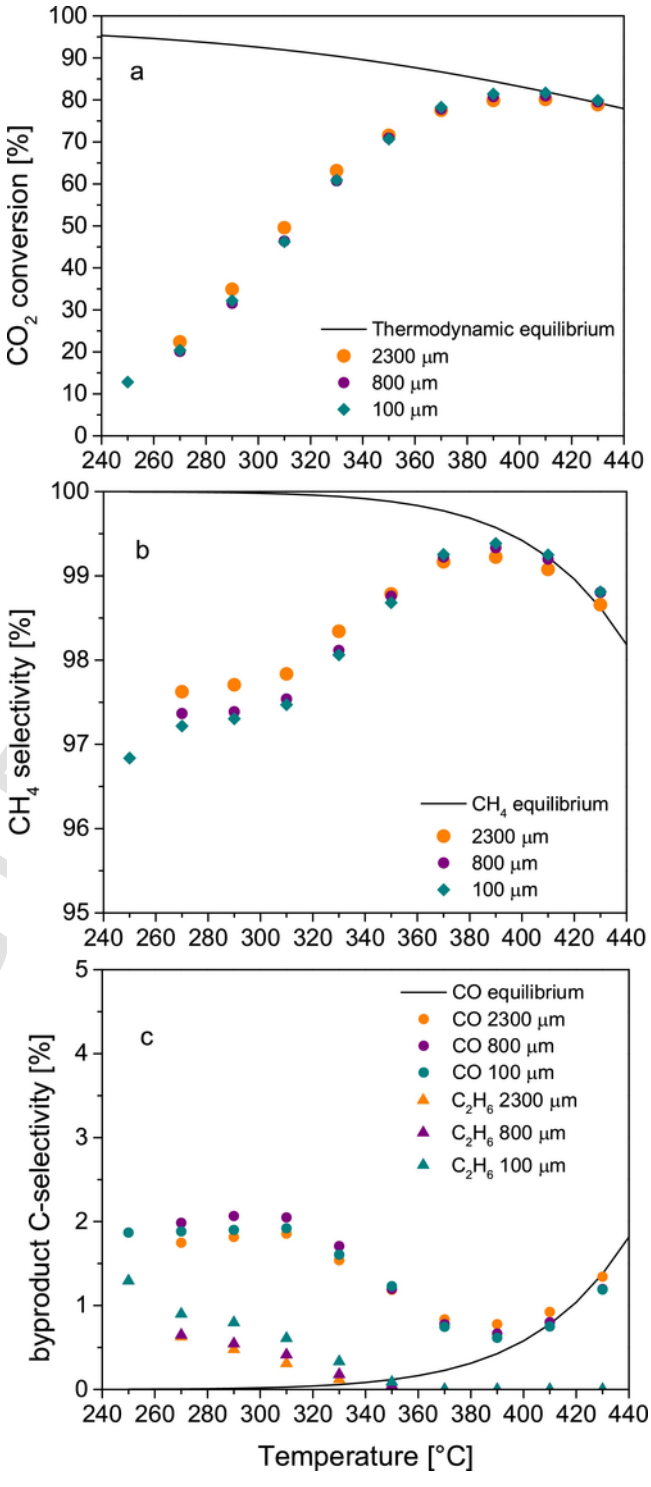


Fig. 12. CO_2 conversion (a) and CH_4 selectivity (b) and CO/C_2H_6 selectivity (c) as a function of temperature for 0.5 wt. % Ru homogenously impregnated on γ-Al_2O_3 spheres of 100, 800 and 2300 μm prepared using $Ru(NO)(NO_3)_3$ as precursor.Process conditions: P = 0 barg, H_2/CO_2 = 3.9 mol/mol, GHSV = 5 L(STP)/h/g_{cat}.

ances (always closing within ±5%), defined as the ratio between the amount of converted carbon and the total amount present in the products. More detailed information about the experimental set up may be found elsewhere [7].

In a typical run, 0.375 g of catalytic pellets were loaded into the reactor diluted with inert α-Al_2O_3 of the same granulometry (1:1 volumetric dilution ratio) to avoid hotspots. The temperature of the electric furnace was controlled by a J-type thermocouple placed at the center of the catalytic bed on the reactor axis. At the beginning of each run, the catalyst was reduced in situ in pure hydrogen flow (1.8 L(STP)/h/g_{cat}), at 400 °C for 3 h (heating ramp 2 °C/min) and atmospheric

pressure. The reactor was subsequently cooled to 250 °C and H_2 was substituted with N_2 (5 L(STP)/h/g_{cat}). Nitrogen was in turn slowly replaced by an equal volumetric flowrate of reactive mixture (98% H_2/CO_2 = 3.9 mol/mol, 2% Ar). The catalyst was then conditioned by increasing the temperature up to 350 °C (heating ramp = 1 °C/min) and keeping it constant until CO_2 conversion and CH_4 selectivity reached a steady value. Once the catalyst was conditioned, the temperature was varied stepwise in the range 250–430 °C. Each temperature level was maintained for no less than 2 h, guaranteeing a stable catalytic performance for each step. A test at 350 °C was repeated at lead twice during the run as activity check. After the test, the catalysts have been cooled down in inert atmosphere and treated at room temperature with 2% v/v O_2 in He (1 L(STP)/h/g_{cat}) to allow a representative characterization of the spent catalysts.

3. Results and discussion

3.1. Preparation and characterization of catalysts using $Ru(NO)(NO_3)_3$ precursor

3.1.1. Eggshell catalyst preparation

Fig. 1 shows the catalyst resulting from the impregnation of a 2300 μm γ-Al_2O_3 pellet with a 0.0676 M $Ru(NO)(NO_3)_3$ solution, which concentration was set to obtain a metal loading of 0.5 wt. %. Fig. 1a shows the external surface and the diametric section of the dried pellet, while Fig. 1b reports the same catalyst after the calcination process. As can be observed, the adopted impregnation method spontaneously led to the preparation of eggshell catalysts, with a thickness of the active layer of 230 ± 20 μm, roughly corresponding to 20% of the pellet radius. According to simple volumetric considerations, the local Ru loading on the outer shell was estimated to be around 1 wt. %.

The calcination procedure (5 h at 400 °C in static air, heating ramp 2 °C/min) did not alter the distribution of the active phase in the pellet, and resulted only in a change of color from light brown to black due indicating the oxidation of ruthenium nitrate to RuO_2.

The SEM/EDX measurement of the ruthenium concentration inside the pellet gave the results shown in Fig. 2. The active phase was detected only on the outer shell of the catalyst sphere. The average metal content of 0.8 ± 0.3 wt. %, measured between r/R = 0.85 and 0.95, is in line with the expected metal loading in the active layer of 1 wt. %. The maximum concentration of Ru was found on the outer surface of the pellets, where the loading is as high as 1.5 ± 0.3 wt.%.

Various methods can be deployed to impregnate catalytic particles in eggshell configuration according to the literature. The reported methods are fairly complex and mainly dealing with the preparation of supported cobalt catalysts for the Fischer-Tropsch (FT) synthesis [19–23]. Ruthenium catalysts, normally used with a much lower metal content with respect to FT catalysts, are apparently prepared with similar methods if an eggshell configuration is desired [24,25].

The phenomenon of the "spontaneous" eggshell formation in noble metal catalysts has been firstly observed in the case of Pt/Al_2O_3 catalysts by Maatman [26]. He showed that a chloroplatinc acid solution used to impregnate γ-Al_2O_3 yields eggshell catalyst in a single impregnation step if the total amount of Pt atoms in the solution is lower than the adsorption sites on the support surface. In fact, under these circumstances the solution is rapidly depleted of the metal ions, that are strongly adsorbed onto the outer regions of the pores. As a consequence, the inner pores are then completely filled by a metal-depleted solution. In this way, the metal precursor ends up titrating the support adsorption sites, meaning that it proceeds further into the pores only once all the previous adsorption sites are occupied.

In order to validate this explanation in our specific case, the impregnation process was repeated over already-impregnated 2300 μm pellets. The resulting catalysts (with a ruthenium loading of around 1 wt. %) exhibited an active layer thickness of 616 μm, indicating that a similar fraction of the support volume was impregnated in each impregnation step. Furthermore, when a single impregnation step was used to deposit 1 wt. % of ruthenium onto a γ-Al_2O_3 pellet of 2300 μm (i.e. using a solution with a double Ru concentration with respect to the previous case), the thickness of the active layer resulted to be 585 μm, in good agreement with the value obtained with two consecutive impregnations (supporting material, **Figure S1**). This confirms a strong metal precursor – support interaction which results in the titration of the support sites by the metal ions contained in the impregnating solution.

Many explanations have been provided over the years to describe the strong metal precursor-support interaction, especially in the case of the H_2PtCl_6 solutions used to impregnate γ-Al_2O_3 supports. These include the dissolution of aluminum and the subsequent complexation/precipitation of the metal precursor [27,28] or the so-called "triple-layer" models, which rely on a chemical adsorption mechanism [29]. However, nowadays the generally accepted description of this interaction is the revised physical adsorption model provided by Spieker and Regalbuto [30], which describes the adsorption of metal ions on the catalyst support as a purely physical phenomenon based on coulombic and solvation interactions.

Since the Point of Zero Charge (PZC) of γ-Al_2O_3 is found at a pH value of about 8 and the metal containing impregnating solution has a strongly acidic nature (pH = 0.5), the surface of the alumina support in these conditions should be positively charged and able to adsorb the negatively charged Ru complex. Indeed, we have tried repeating our impregnation method on SiO_2 pellets (S_{BET} = 366 m^2/g, V_p = 0.82 cm^3/g, average d_p = 8.2 nm), which has its PZC at a pH value of about 3. In this case, the support surface has an almost neutral charge in the impregnating solution conditions, and the metal - support interaction is rather weak. Hence, fully impregnated catalysts were obtained (supporting material, **Figure S2**).

The impregnation of γ-Al_2O_3 with excess solution was also investigated to assess the possibility to prepare a homogeneous 0.5 wt. % Ru/γ-Al_2O_3 catalyst using the wet impregnation method. For this purpose, the alumina spheres have been soaked in a large excess of solution having the same ruthenium concentrations used in the dry impregnation to obtain a nominal metal loading of 0.5 or 1 wt.%. Fully impregnated samples have been obtained after 20 min of soaking (the reader is referred to **Figure S3a** of the supporting material for a more detailed description of the experiment and results). However, in this case the homogeneously impregnated pellets had a higher ruthenium content with respect to the desired 0.5 wt. %, determined by the larger availability of Ru in the solution. This result points out that wet impregnation is not a suitable method to prepare homogeneous Ru/γ-Al_2O_3 catalyst with controlled Ru-loadings.

3.1.2. Homogeneously impregnated catalyst preparation

Maatman [26] and Mang et al. [29] report that a uniform distribution of a metal precursor which interacts strongly with the catalyst support can be obtained through the addition of an inorganic acid in the impregnating solution. The role of the acid was believed to be that of a competitive adsorbate, able to strongly adsorb onto the support sites, thus favoring the penetration of the metal precursor into the pores of the support. According to the revised physical adsorption model suggested in [30], the role of the introduced acid is to change the electric charge of the support surface by modifying the pH of the solution, thus tuning the strength of the metal precursor - support interaction.

In our specific case the impregnating solution is already strongly acidic (pH = 0.5) and a possible solution could be to introduce a base in the solution in order to increase the pH towards the PZC of the support, so to have a less positively charged surface which will interact less with the metal complex. In these conditions, the metal precursor

UNCORRECTED PROOF

should be evenly deposited along the pellet radius. However, the use of a basic agent could reveal problematic, as it could cause the undesired precipitation of the metal precursor, which is effectively stabilized only in acidic solutions. An alternative option could be the addition of an acid to further decrease the pH of the solution. In these conditions, even if the alumina surface remains positively charged, the surface potential is expected to decrease due to the high ionic strength of the solution, resulting in a decrease of the strength of the metal precursor – support interactions and thus yielding homogeneously impregnated pellets.

On these grounds, instead of diluting the desired volume of commercial $Ru(NO)(NO_3)_3$ with deionized water, solutions of deionized water and nitric acid in variable ratios have been used, keeping the metal concentration constant in the impregnating solutions. The thickness of the catalytic layer in the resulting catalyst, prepared on 2300 μm γ-Al_2O_3 as to obtain a nominal metal loading of 0.5 wt%, are shown in Fig. 3. For a better identification of the active shell, a similar figure is reported in the supporting material with the calcined samples (**Figure S4a**). The reader must be aware that the commercial Ru nitrosyl nitrate solution used in this work already contains amounts of HNO_3 to guarantee the complete dissolution of the metal precursor; hence, the actual HNO_3/Ru ratio in the impregnating solution is higher with respect to what reported in Fig. 3 and **S4a**.

It is evident that a progressive increase in the amount of nitric acid in the impregnating solution causes a progressive increase in the thickness of the catalytic layer of the pellet. Furthermore, a linear dependence can be observed between the extent of Ru penetration in the pellet (i.e. the thickness of the impregnated shell) and the HNO_3/Ru molar ratio, until no inert core remains at an added HNO_3/Ru ratio of about 20. However, the sample prepared with HNO_3/Ru = 20, shows a darker tone at the outer layer, indicating that despite the metal is present along the whole pellet radius, it is not deposited homogeneously throughout the pellet. Hence, the amount of acid was further increased reaching a ratio HNO_3/Ru ratio of 117, obtained by diluting the commercial solution of the precursor to the required volume only with HNO_3. In this case no color differences were observed throughout the pellet, suggesting the absence of Ru concentration gradients along the pellet radius. To verify the effective metal concentration, SEM/EDX analyses were performed and the results are reported in Fig. 4. As can be observed, ruthenium was detected along the whole pellet radial coordinate and the estimated metal content is reasonably constant and in good agreement with the theoretical value of 0.5 wt. %.

Notably, γ-Al_2O_3 can be soluble in highly acidic environments, leading to the embrittlement of the support, especially after the thermal treatment of the catalyst. Furthermore, the partial dissolution of the support may result in a subsequent re-deposition on the catalyst surface, with the risk of covering the active phase [31]. In order to investigate the effect of the acid introduction, the homogenously impregnated catalysts obtained using molar ratios of added HNO_3/Ru equal to 20 and 117, were either calcined in static air at 400 °C or reduced in H_2 flow at 400 °C to evaluate the effects of oxidizing and reducing treatments at high temperatures. The pellets are shown in Fig. 5 after drying at 120 °C, after calcination and after reduction. At variance to the catalyst prepared without any extra HNO_3 addition (shown in its calcined form in Fig. 1a), the pellets decolored completely after the calcination process (Fig. 5b and e), suggesting a loss of the active phase. As a matter of facts, SEM/EDX analysis confirmed the absence of ruthenium in the calcined catalysts prepared at a HNO_3/Ru molar ratio higher than 20. Furthermore, when a CO_2 methanation test was attempted over the calcined homogenously impregnated pellets, no catalytic activity was measured.

The loss of active phase is possibly due to the formation of the volatile RuO_4 (instead of the less oxidized and more stable form, RuO_2) at high temperatures in oxidizing environments [8]. Indeed, a more severe oxidation process can be effectively enhanced in the homogeneously impregnated pellets by the large presence of residual nitrate group onto the catalyst surface, as a result of the preparation procedure.

Unfortunately, the sharp cut of the calcined spherical pellet by a razor blade proved to be much more difficult for the sample prepared with the largest amount of HNO_3, resulting in uneven cross-cut surfaces. Indeed, in these conditions the calcination process caused the embrittlement of the alumina support, possibly because of the high temperature leaching of aluminum in presence of residual nitric acid on the catalyst surface.

Notably, the samples reduced at 400 °C in H_2 (shown in Figs. 5c and f) retain the original coloration, as well as the metallic loading was retained at high temperature in reducing environments. In the case of the sample shown in Fig. 5c, obtained using less acid, the dark color assumed upon calcination stresses the differences in the local concentration along the pellet radius, which become even more evident with respect to the dried sample (Fig. 5a). This is not the case for the sample obtained using a higher content of acid (Fig. 5f). However, as observed for the calcined samples, the reduced sample prepared at HNO_3/Ru ratio of 117 showed an irregular surface of the cut, indicating that the mechanical properties of the pellet appear to be affected by high temperature treatment after the exposure to concentrated acidic solutions.

In order to evaluate a possible effect of the acid introduction on the dispersion of the metal, TEM images of both the 2300 μm eggshell catalyst (1 wt. % Ru on the shell, HNO_3/Ru = 0) and the homogeneously impregnated 2300 μm catalyst (0.5 wt. %, HNO_3/Ru = 117) are shown in Fig. 6 after reduction in H_2 at 400 °C and exposure to 2% O_2 at room temperature. The average ruthenium particle size is very similar in the two samples, yielding sub nanometric crystallites and indicating a very high dispersion of the metallic phase. This evidence is confirmed by H_2 chemisorption experiments on the same samples. Indeed, the eggshell sample and the homogeneously impregnated sample show a very similar metal dispersion (40 and 41%, respectively), suggesting a negligible effect of the acid addition on the metal particle size. The average metal particle diameter has been evaluated from the dispersion values using the relation reported in [12–14]. A value of 2.1 nm was obtained in the case of the eggshell catalyst, while a value of 2.0 nm was obtained for the homogeneously impregnated sample. These values are in reasonable agreement with data obtained by TEM (~1 nm for both samples), and confirm the very similar metal dispersion of these samples in spite of their different preparation methods.

The almost identical dispersion of these samples is possibly due to the removal of aluminum ions from the surface of the support in presence of highly acidic solutions which creates a highly defective surface on which ruthenium can be more easily anchored. A similar effect – though with a lower metal dispersion – was observed by Mieth and Schwarz [32] in the case of γ-Al_2O_3-supported ruthenium catalysts with metal loadings in the range 0.76–5 wt. %.

It is worth noting that the same analyses carried out in the case of the 2300 μm alumina have been repeated with similar results in the case of the smaller 800 μm pellets, prepared using the same preparation method. In this case, the obtained active layer thickness of the "spontaneous" eggshell catalyst was of 75 ± 30 μm, corresponding to about 20% of the pellet radius, the same relative percentage obtained in the case of the 2300 μm γ-Al_2O_3. Furthermore, also in the case of the 800 μm microspheres, homogeneously impregnated samples were obtained by introducing HNO_3 in the impregnating solution at a HNO_3/Ru ratio of 117.

The catalyst prepared using the 100 μm thick γ-Al_2O_3 powders were assumed homogeneously impregnated even when no acid was introduced during the preparation, based on the higher accessibility of the support adsorption sites.

UNCORRECTED MANUSCRIPT

3.2. Preparation and characterization of catalysts using $RuCl_3$ precursor

The preparation experiments have been repeated also using ruthenium chloride as precursor. The impregnated 2300 μm pellet is shown in Figs. 7a and b in its dried and calcined form, respectively. The thickness of the active layer, which is not affected by the calcination process (as previously observed also in the case of the nitrate precursor) is of 40 ± 8 μm, corresponding to less than 4% of the pellet radius. Notably, the active layer thickness obtained in this case is much smaller with respect to that obtained starting from a $Ru(NO)(NO_3)_3$ precursor (see Fig. 1a and b for comparison). Hence the local concentration of the active phase in this case is higher than in the case of the $Ru(NO)(NO_3)_3$, reaching about 4.7 wt. %. This difference is attributed to the presence of HNO_3 in the commercial solution of nitrosyl nitrate we used as precursor, which – as previously observed – enhances the penetration of the metal into the catalyst pores by lowering the strength of the metal precursor – support interaction.

The difference between the two precursors results also in longer times required to obtain a homogeneously impregnated pellet when using a large excess of $RuCl_3$ solution with the same concentration (compare **Figures S3a** and **S3b** in supporting material).

Following the same approach used in the case of the nitrate precursor, to tune the thickness of the impregnated layer, the impregnating solution has been acidified with various amounts of HCl while keeping the ruthenium concentration constant. Fig. 8 reports the relationship between the catalyst shell thickness and the acid/precursor molar ratio (see **Figure S4b** in the supporting material for the corresponding plot with calcined samples). As expected, the higher is the amount of acid introduced, the higher is the average thickness of the active layer. However, in this case, the increase in the catalytic layer thickness with the amount of added acid is less pronounced with respect to what obtained with ruthenium nitrate precursor (compare Fig. 8 with Fig. 3). As a result, higher amounts of acid have to be introduced to obtain the same eggshell thickness obtained in the case of the ruthenium nitrate precursor. Nevertheless, uniformly impregnated pellets were obtained at an $HCl/RuCl_3$ molar ratio of 143 but, as suggested by the trend lines reported in Fig. 8, the same result could have been obtained using a smaller amount of HCl, corresponding to a HCl/Ru ratio of 53.

In the case of the $RuCl_3$ precursor, the concentration profile of Ru along the pellet radial coordinate could not be obtained via SEM/EDX because the main fluorescence bands of Cl and Ru have very similar values, and a reliable quantification using secondary peaks is not viable due to the relatively low metal loading.

Fig. 9 shows the homogeneously impregnated pellets (prepared at HCl/Ru molar ratios of 53 and 143) in their dried, calcined and reduced form. At variance to what observed in the case of the nitrate precursor, the dried pellet prepared with the lower amount of acid (Fig. 9a) does not show any sign of internal concentration gradients upon visual inspection and its mechanical properties are also unaffected. On the contrary, the uniformly impregnated pellet obtained in the most severe conditions (Fig. 9d) proved difficult to cut evenly, suggesting that the strong acidity of the impregnating solution caused a worsening of the mechanical properties already at relatively low temperatures.

After the calcination process both chloride samples turned grey (Fig. 9b and e). This suggests that the samples were able to retain at least a part or their metal content, probably due to the lack of the strongly oxidizing nitrate groups which can generate the volatile RuO_4 species. Nevertheless, in both cases the calcined pellets appear darker on the outer surface with respect to the inner part, suggesting a migration of the metal on the outer surface of the pellet at high temperatures in oxidizing conditions.

The homogeneously impregnated pellet prepared from the chloride precursor were able to retain their metal content also after the reducing treatment (Fig. 9c and f), as indicated by the gray color. Also, in this case, at variance to what observed after the calcination treatment, no indications of rearrangements/loss of the active phase were observed. This confirms that $Ru/\gamma\text{-}Al_2O_3$ catalysts are more stable in reducing conditions than under oxidizing atmospheres.

3.3. Catalytic activity tests

3.3.1. Experiments with 100 μm catalysts

Fig. 10 shows the CO_2 conversion and CH_4 selectivity as a function of time on stream (T.o.S.) in the first 150 h on stream for 0.5 wt. % Ru-based catalysts prepared on the 100 μm support using $Ru(NO)(NO_3)_3$ or $RuCl_3$ aqueous solutions without extra acid. The catalyst prepared starting from the nitrosyl nitrate precursor shows steady state performance since the first hours on stream. Activity checks at higher T.o.S. also confirmed the stability of this catalytic system in the investigated process conditions. At variance, the catalyst prepared with the chloride precursor shows a slow increase with time of both CO_2 conversion rate and CH_4 selectivity. As a result, steady state performance is achieved only after 150 h on stream.

We attribute the slow increase of CO_2 conversion and CH_4 selectivity of the chloride sample to the poisoning effect of residual halogen ions on the catalyst surface, which are progressively removed. Indeed, Ru-based catalysts prepared from $RuCl_3$ are known to retain substantial amounts of chlorine even after a thermal pretreatment [17], and the water formed by the Sabatier reaction (Eq. 1) could react with chloride ions, thus producing HCl that is removed by the outlet gas stream [33]. As a matter of fact, we found that the pH of the aqueous phase condensed downstream of the reactor has values around 1 in the first hours on stream, but progressively increases with time on stream until reaching neutral values after about 150 h on stream, when a stable catalytic performance was measured (pH values as a function of T.o.S. are reported in **Figure S5** of the supporting material for the test reported in Fig. 10).

The reasons why chloride ions limit the catalyst activity and worsen the selectivity to methane are different. CO_2 conversion rate is depressed because Cl^- ions hinder the adsorption of the reactants, while CO selectivity is increased because chlorine weakens the metal CO-bond. Indeed, it is accepted in the literature that CO is an intermediate in the Sabatier reaction [34–36] and this species is strongly adsorbed on the metallic phase via π back-bonding. Since chlorine has a high electronegativity it can retain the electrons of the metal, which are less available for the π back-donation, thus weakening the metal–CO bond and increasing the possibility of its desorption prior to its complete hydrogenation to methane.

Once the conditioning transient is over, the catalytic performance of the two samples is similar, even if the sample prepared from $RuCl_3$ shows slightly lower CO_2 conversion (66 vs 71%) and CH_4 selectivity (98% vs 99%). STEM results (supporting material, **Figure S6**) indicate a very similar metal particle size distribution in the two samples. The average particle size is in both cases between 0.9 and 1 nm. Hence, the reason of the slight difference in activity and selectivity could be due to the residual presence of residual chloride ions on the catalyst surface. In any case, a rationale to employ $RuCl_3$ as metal precursor – given that the catalyst morphology and steady state activity is comparable to those obtained with the nitrate precursor – is provided by its lower price with respect to the nitrate salt. The long conditioning time required for the Cl^- ions removal from the catalyst surface could be avoided, at the expenses of a more complicated synthesis procedure [37,38].

UNCORRECTED PROOF

3.3.2. Experiments with powdered eggshell and homogeneously impregnated catalysts

With the purpose of evaluating whether the acid introduction has an effect on the reactivity of the catalytic systems, the 2300 μm eggshell and homogeneously impregnated catalysts prepared using $Ru(NO)(NO_3)_3$ with (HNO_3/Ru = 117) or without HNO_3 have been tested after grounding and sieving below 106 μm to ensure kinetically controlled conditions. The introduction of the acid influenced neither the conditioning transient of the catalyst (data shown in supplementary materials, **Figure S7**), as a stable performance is reached within the first hour for both catalysts prepared from the nitrate precursor, nor their steady state performance.

The steady performance in term of CO_2 conversion, CH_4 selectivity and byproduct selectivity is reported in Fig. 11a-c, respectively, as a function of temperature. The results obtained on the ruthenium catalyst directly impregnated onto 100 μm alumina powders as well as the performance expected at thermodynamic equilibrium are also reported for comparison.

The CO_2 conversion increases with temperature until the thermodynamic equilibrium composition is approached at a temperature of about 410 °C (Fig. 11a). At higher temperatures, a decrease in the CO_2 conversion is observed, as predicted by thermodynamics. The selectivity to methane is always above 97% and it follows a trend similar to CO_2 conversion, i.e. it increases with temperature until the equilibrium composition is reached, and then starts decreasing with increasing temperature (Fig. 11b). The byproducts selectivity is also reported (Fig. 11c). CO is the most abundant byproduct, and it is present in the whole investigated temperature range. Interestingly, its selectivity appears to be rather constant between 250 and 310 °C, while its concentration in the products decreases at higher temperatures prior to reach the equilibrium composition. Ethane is detected only at temperatures below 350 °C and its concentration at the reactor outlet decreases linearly with increasing temperature. The maximum observed selectivity is equal to 1.3% at the lowest investigated temperature of 250 °C. Notably, the presence of C_2H_6 can be explained considering the occurrence of some chain growth reactions, according to a Fischer-Tropsch chain growth mechanism, for which ruthenium is known to be an active catalyst [39,40]. The low selectivity towards C_{2+} species observed in our products is due to the low pressures and relatively high temperatures used in this work, at which hydrogenation processes are favored over C—C bond formation steps.

As can be observed from the almost superimposed data reported in Fig. 11, recalling that the dispersion between the eggshell catalysts and the homogenously impregnated catalysts is the same (Section 3.1.2, Fig. 6), it is reasonable to conclude that the acid introduction has a negligible effect on the catalytic performance.

In the case of the chloride precursor, a similar comparison has been performed on the powdered 2300 μm pellets (the steady state performance of the two catalysts is reported in the supplementary material, **Figure S8**). The homogeneously impregnated pellet (prepared with HCl/Ru ratio of 143) required more than 250 h of conditioning to reach a stable performance, due to the large amounts of Cl^- ions introduced during the preparation. Furthermore, the catalyst prepared with the hydrochloric acid addition showed a lower catalytic activity and exhibited a deactivation behavior from the temperature of 370 °C. This indicates that, at variance to what observed for HNO_3, the addition of large amounts of HCl has a detrimental effect on the catalytic activity. Hence, further investigation the assessment of the presence of internal diffusional limitation has been carried out only on the homogenous samples prepared from the nitrate precursor.

3.3.3. Assessment of internal mass transfer limitations

Fig. 12 reports the CO_2 conversion and product selectivity plots for the homogeneously impregnated 100, 800 and 2300 μm 0.5 wt. % Ru/Al_2O_3 catalyst. 800 and 2300 μm pellets have been prepared from the nitrate precursor aqueous solution containing HNO_3 with a HNO_3/Ru ratio of 117. The curves of conversion and selectivity for the three samples are almost superimposed, indicating that the pellet diameter has no effect on the catalytic performance. Furthermore, to rule out any difference due to the preparation of different batches of catalysts, each sample has been confronted with its powdered form, and identical results have been obtained both in conversion and selectivity (supporting materials, **Figure S9**). These results prove that the pellets of the three investigated diameters are all working in a kinetically controlled regime, and the internal diffusional limitations can be safely neglected when using these catalysts.

Given these premises, it is possible to evaluate the characteristic length of diffusion as the ratio between the volume and the external surface of the catalytic particles, which corresponds to one sixth of the diameter in the case of fully impregnated spherical pellets. In the most stringent conditions for internal diffusional limitations evaluated in this work (i.e. 2300 μm pellets) this value corresponds to 383 μm. Therefore, it is possible to conclude that the presence of internal diffusional limitations can be ruled out on 0.5 wt. % Ru/Al_2O_3 catalysts when using pellets with a characteristic diffusion length shorter than 383 μm.

4. Conclusions

In this work 100, 800 and 2300 μm γ-Al_2O_3 pellets have been impregnated with a ruthenium nitrosyl nitrate or a ruthenium chloride solution with the aim of synthesizing pellets with an overall metal loading of 0.5 wt. %. The adopted impregnation method led to the preparation of eggshell catalysts on pellets bigger than 100 μm due to the strong metal precursor-support interaction. However, by introducing an inorganic acid in the impregnating solution, it is possible to effectively tune the shell thickness of the eggshell layer, until obtaining homogeneously impregnated pellets. In fact, a linear correlation has been evidenced between the active layer thickness and the acid/metal molar ratio in the impregnating solution.

Notably, the addition of even large amounts of HNO_3 to Ru nitrosyl nitrate solutions did not affect the catalytic performance, while the use of HCl added to Ru chloride precursor resulted in catalyst deactivation at higher temperatures. In both cases, a loss of mechanical strength was observed when large amounts of acid have been used.

The homogeneously impregnated pellets prepared with a $Ru(NO)(NO_3)_3$/HNO_3 solution have been tested in a fixed bed configuration in order to assess the onset of intraporous diffusional limitations, which have not been observed even with the 2300 μm homogeneously impregnated pellets containing 0.5 wt. % Ru. Hence, we can conclude that internal diffusional limitations are not present up to a characteristic length of diffusion of 383 μm and that 0.5 wt. % Ru/ γ-Al_2O_3 catalysts are appropriate for industrial operations. Experiments with catalysts impregnated with higher Ru contents are currently undergoing in our labs.

References

[1] E.A. Quadrelli, G. Centi, J.L. Duplan, S. Perathoner, Carbon dioxide recycling: emerging large-scale technologies with industrial potential, ChemSusChem 4 (2011) 1194–1215, https://doi.org/10.1002/cssc.201100473.

[2] IEA, World Energy Outlook 2017, Int. Energy Agency, 2017.

[3] K. Ghaib, F.Z. Ben-Fares, Power-to-Methane: a state-of-the-art review, Renew. Sustain. Energy Rev. 81 (2018) 433–446, https://doi.org/10.1016/j.rser.2017.08.004.

[4] P. Frontera, A. Macario, M. Ferraro, P. Antonucci, Supported catalysts for CO_2 methanation: a review, Catalysts 7 (2017) 59, https://doi.org/10.3390/catal7020059.

UNCORRECTED PROOF

[5] S. Rönsch, J. Schneider, S. Matthischke, M. Schlüter, M. Götz, J. Lefebvre, P. Prabhakaran, S. Bajohr, Review on methanation - from fundamentals to current projects, Fuel166 (2016) 276–296, https://doi.org/10.1016/j.fuel.2015.10.111.

[6] G.D. Weatherbee, C.H. Bartholomew, Hydrogenation of CO_2 on group VIII metals. IV. Specific activities and selectivities of silica-supported Co, Fe, and Ru, J. Catal. 87 (1984) 352–362, https://doi.org/10.1016/0021-9517(84)90196-9.

[7] L. Falbo, M. Martinelli, C.G. Visconti, L. Lietti, C. Bassano, P. Deiana, Kinetics of CO_2 methanation on a Ru-based catalyst at process conditions relevant for Power-to-Gas applications,, Appl. Catal. B Environ. 225 (2018) 354–363, https://doi.org/10.1016/j.apcatb.2017.11.066.

[8] C. Janke, M.S. Duyar, M. Hoskins, R.J. Farrauto, Catalytic and adsorption studies for the hydrogenation of CO_2 to methane, Appl. Catal. B Environ. 152–153 (2014) 184–191, https://doi.org/10.1016/j.apcatb.2014.01.016.

[9] R. Farrauto, Y. Liu, W. Ruettinger, O. Ilinich, L. Shore, T. Giroux, Precious metal catalysts supported on ceramic and metal monolithic structures for the hydrogen economy, Catal. Rev. - Sci. Eng. 49 (2007) 141–196, https://doi.org/10.1080/01614940701220496.

[10] M. Frey, T. Romero, A.C. Roger, D. Edouard, Open cell foam catalysts for CO_2 methanation: presentation of coating procedures and in situ exothermicity reaction study by infrared thermography, Catal. Today 273 (2016) 83–90, https://doi.org/10.1016/j.cattod.2016.03.016.

[11] C. Fukuhara, K. Hayakawa, Y. Suzuki, W. Kawasaki, R. Watanabe, A novel nickel-based structured catalyst for CO_2 methanation: a honeycomb-type Ni/CeO_2 catalyst to transform greenhouse gas into useful resources, Appl. Catal. A Gen. 532 (2017) 12–18, https://doi.org/10.1016/j.apcata.2016.11.036.

[12] C.H. Yang, J.G. Goodwin, Reversible chemisorption on highly dispersed Ru catalysts, J. Catal. 78 (1982) 182–187, https://doi.org/10.1016/0021-9517(82)90297-4.

[13] B. Chen, J.G. Goodwin, Isotopic transient kinetic analysis of CO hydrogenation on Cu-modified Ru/SiO2, J. Catal. 158 (1996) 511–520, https://doi.org/10.1006/jcat.1996.0050.

[14] J. Okal, M. Zawadzki, L. Kepiński, L. Krajczyk, W. Tylus, The use of hydrogen chemisorption for the determination of Ru dispersion in Ru/γ-alumina catalysts, Appl. Catal. A Gen. 319 (2007) 202–209, https://doi.org/10.1016/j.apcata.2006.12.005.

[15] J.G. Goodwin Jr, Characterization of highly dispersed ruthenium catalysts by chemisorption, J. Catal. 68 (1981) 227–232.

[16] S.Y. Chin, O.S. Alexeev, M.D. Amiridis, Preferential oxidation of CO under excess H_2 conditions over Ru catalysts, Appl. Catal. A Gen. 286 (2005) 157–166, https://doi.org/10.1016/j.apcata.2005.02.031.

[17] P.G.J. Koopman, A.P.G. Kieboom, H. van Bekkum, Characterization of ruthenium catalysts as studied by temperature programmed reduction, J. Catal. 69 (1981) 172–179, https://doi.org/10.1016/0021-9517(81)90139-1.

[18] J. Wellenbuscher, M. Muhler, W. Mahdi, U. Sauerlandt, J. Schutze, G. Ertl, R. Schlogl, Ruthenium supported on zeolite A: preparation and characterisation of a stable catalyst for ammonia synthesis, Catal. Lett. 25 (1994) 61–74, https://doi.org/10.1007/BF00815416.

[19] E. Iglesia, S.L. Soled, J.E. Baumgartner, S.C. Reyes, Synthesis and catalytic properties of eggshell cobalt catalysts for the fischer-tropsch synthesis, J. Catal. 153 (1995) 108–122, https://doi.org/10.1006/jcat.1995.1113.

[20] Y.Q. Zhuang, M. Claeys, E. Van Steen, Novel synthesis route for egg-shell, egg-white and egg-yolk type of cobalt on silica catalysts, Appl. Catal. A Gen. 301 (2006) 138–142, https://doi.org/10.1016/j.apcata.2005.11.029.

[21] H.P.C.E. Kuipers, M.J. Reynhout, US 2008/0255257 A1 Process for Making an Egg Shell FT Catalyst, 2008.

[22] J.T. Wolan, A. Gardezi, US 2012/0149559 A1 Eggshell Catalyst and Method of Its Preparation, 2012.

[23] L. Fratalocchi, C.G. Visconti, L. Lietti, E. Tronconi, U. Cornaro, S. Rossini, A novel preparation method for "small" eggshell $Co/\gamma\text{-}Al_2O_3$ catalysts: a promising catalytic system for compact Fischer-Tropsch reactors, Catal. Today 246 (2015) 125–132, https://doi.org/10.1016/j.cattod.2014.09.020.

[24] M. Yang, Y. Sun, A.H. Xu, X.Y. Lu, H.Z. Du, C.L. Sun, C. Li, Catalytic wet air oxidation of coke-plant wastewater on ruthenium-based eggshell catalysts in a bubbling bed reactor, Bull. Environ. Contam. Toxicol. 79 (2007) 66–70, https://doi.org/10.1007/s00128-007-9150-6.

[25] E.H. Cho, K.Y. Koo, H.W. Lee, Y.K. Park, W.L. Yoon, C.H. Ko, Preparation of egg-shell-type Ni/Ru bimetal alumina pellet catalysts: steam methane reforming for hydrogen production, Int. J. Hydrogen Energy42 (2017) 18350–18357, https://doi.org/10.1016/j.ijhydene.2017.04.170.

[26] R. Maatman, How to make a more effective platinum-alumina catalyst, Ind. Eng. Chem. 51 (1959) 913–914, https://doi.org/10.1021/ie50596a029.

[27] E. Santacesaria, S. Carrà, I. Adami, Adsorption of hexachloroplatinic acid on γ-Alumina, Ind. Eng. Chem. Prod. Res. Dev. 16 (1977) 41–44, https://doi.org/10.1021/i360061a007.

[28] L.L. Murrell, D.J.C. Yates, Preparation of highly-dispersed ruthenium on magnesium oxide supports: comments on the advantages of non-aqueous catalyst preparations, Stud. Surf. Sci. Catal. 3 (1979) 307–319, https://doi.org/10.1016/S0167-2991(09)60221-4.

[29] T. Mang, B. Breitscheidel, P. Polanek, H. Knözinger, Adsorption of platinum complexes on silica and alumina: preparation of non-uniform metal distributions within support pellets, Appl. Catal. A Gen. 106 (1993) 239–258, https://doi.org/10.1016/0926-860X(93)80180-X.

[30] W.A. Spieker, J.R. Regalbuto, A fundamental model of platinum impregnation onto alumina, Chem. Eng. Sci. 56 (2001) 3491–3504, https://doi.org/10.1016/S0009-2509(01)00052-5.

[31] R.J. Fenoglio, W. Alvarez, G.M. Nuñez, D.E. Resasco, Interactions of the impregnating solution with the support during the preparation of Rh/TiO2 catalysts, in: G. Poncelet, P.A. Jacobs, P. Grange, B. Delmon (Eds.), Prep. Catal. V, Elsevier Science Publishers B.V., Amsterdam, 1991, pp. 77–86, https://doi.org/10.1016/S0167-2991(08)64574-7.

[32] J.A. Mieth, J.A. Schwarz, Effects of alumina dissolution and metal ion buffering on the dispersion of alumina supported nickel and ruthenium catalysts, Appl. Catal. 55 (1989) 137–149, https://doi.org/10.1016/S0166-9834(00)82324-6.

[33] G. Garbarino, D. Bellotti, P. Riani, L. Magistri, G. Busca, Methanation of carbon dioxide on Ru/Al_2O_3 and Ni/Al_2O_3 catalysts at atmospheric pressure: catalysts activation, behaviour and stability, Int. J. Hydrogen Energy40 (2015) 9171–9182, https://doi.org/10.1016/j.ijhydene.2015.05.059.

[34] M. Marwood, R. Doepper, M. Prairie, A. Renken, Transient drift spectroscopy for the determination of the surface reaction kinetics of CO_2 methanation, Chem. Eng. Sci. 49 (1994) 4801–4809, https://doi.org/10.1016/S0009-2509(05)80060-0.

[35] X. Wang, Y. Hong, H. Shi, J. Szanyi, Kinetic modeling and transient DRIFTS–MS studies of CO_2 methanation over Ru/Al_2O_3 catalysts, J. Catal. 343 (2016) 185–195, https://doi.org/10.1016/j.jcat.2016.02.001.

[36] G. Garbarino, D. Bellotti, E. Finocchio, L. Magistri, G. Busca, Methanation of carbon dioxide on Ru/Al_2O_3: catalytic activity and infrared study, Catal. Today 277 (2016) 21–28, https://doi.org/10.1016/j.cattod.2015.12.010.

[37] Q. Zheng, R.J. Farrauto, A. Chau Nguyen, Adsorption and methanation of flue gas CO_2 with dual functional catalytic materials: a parametric study, Ind. Eng. Chem. Res. 55 (2016) 6768–6776, https://doi.org/10.1021/acs.iecr.6b01275.

[38] S. Wang, E.T. Schrunk, H. Mahajan, R.J. Farrauto, The role of ruthenium in CO_2 capture and catalytic conversion to fuel by dual function materials (DFM), Catalysts 7 (2017) 88, https://doi.org/10.3390/catal7030088.

[39] D.L. King, A Fischer-Tropsch study of supported ruthenium catalysts, J. Catal. 51 (1978) 386–397, https://doi.org/10.1016/0021-9517(78)90277-4.

[40] E. Iglesia, S.L. Soled, R.A. Fiato, Fischer-Tropsch synthesis on cobalt and ruthenium. Metal dispersion and support effects on reaction rate and selectivity, J. Catal. 137 (1992) 212–224, https://doi.org/10.1016/0021-9517(92)90150-G.

UNCORRECTED PROOF